

BIOTIC IMPACT OF EOCENE THERMAL MAXIMUM 2 IN A SHELF SETTING (DABABIYA, EGYPT)

Peter STASSEN¹⁾, Etienne STEURBAUT^{1,2)}, Abdel-Mohsen M. MORSI³⁾,
Peter SCHULTE⁴⁾ & Robert P. SPEIJER¹⁾

¹⁾ Department of Earth and Environmental Sciences, KU Leuven, Celestijnenlaan 200E, B-3001, Leuven, Belgium;

²⁾ Department of Paleontology, Royal Belgian Institute of Natural Sciences, Vautierstraat 29, B-1000, Brussels, Belgium;

³⁾ Department of Geology, Faculty of Science, Ain Shams University, 11566 Cairo, Egypt;

⁴⁾ GeoZentrum Nordbayern, Universität Erlangen, Schlossgarten 5a, D-91054 Erlangen, Germany;

^{†)} Corresponding author, peter.stassen@ees.kuleuven.be

KEYWORDS

Eocene thermal maximum 2
carbon isotopes
hyperthermal
foraminifera
ostracodes
Egypt

ABSTRACT

The Paleocene-Eocene thermal maximum (PETM) initiated a global biotic event with major evolutionary impacts. Since a series of minor $\delta^{13}\text{C}$ and $\delta^{18}\text{O}$ excursions, indicative of hyperthermals, now appears to characterize early Eocene climate, it remains to be investigated how the biosphere responded to these warming events. We studied the Esna Formation at Dababiya (Nile Basin, Egypt), in order to identify Eocene thermal maximum 2 (ETM-2) and to evaluate the foraminiferal and ostracode patterns. The studied interval generally consists of gray-brown marls and shales and is interrupted by a sequence of deviating lithologies, representing an early Eocene Egyptian environmental perturbation that can be linked to ETM-2. The ETM-2 interval consists of brownish shales (bed 1) to marls (bed 2) at the base that grade into a foraminifera-rich chalky limestone (bed 3) at the top. This conspicuous white limestone bed forms the base of the Abu Had Member. A distinct negative $\delta^{13}\text{C}$ excursion of approximately 1.6‰ is recorded encompassing this interval and a second negative $\delta^{13}\text{C}$ shift of 1‰ occurs 5 m higher. These two isotope events are situated respectively in the basal and lower part of the calcareous nannoplankton zone NP11 and appear to correlate with the H1 and H2(?) excursions observed in the deep-sea records. The lower $\delta^{13}\text{C}$ excursion is associated with benthic foraminiferal and ostracode changes and settlement of impoverished anomalous foraminiferal (planktic and benthic) assemblages, indicating a transient environmental anomaly, disrupting the entire marine ecosystem during ETM-2. Our observations indicate some similarities between the sedimentary and biotic expressions of ETM-2 and the PETM at Dababiya, pointing to similar processes operating in the Egyptian Basin during these global warming events.

1. INTRODUCTION

The well-studied Paleocene-Eocene thermal maximum (PETM, also known as Eocene thermal maximum 1 or ETM-1) is the most extreme of a series of rapid global warming events or hyperthermals, that occurred during the long-term early Paleogene warming (Zachos et al., 2008). Less pronounced transient warming events recently described are the Latest Danian Event (LDE, Bornemann et al., 2009; Westerhold et al., 2011) and Eocene thermal maximum 2 (ETM-2, Lourens et al., 2005; Stap et al., 2010). These hyperthermals are associated with massive injections of ^{13}C -depleted carbon into the ocean-atmosphere system, and are registered as negative carbon isotope excursions (CIE's) in the sedimentary record. At Walvis Ridge, ETM-2 (representing the H1 isotope event of Cramer et al., 2003) is characterized by a CIE of -1.4‰ in association to a 3 °C deep-sea warming, with a more gradual CIE-onset in comparison to the PETM (Stap et al., 2010). It is positioned stratigraphically within the basal part of calcareous nannoplankton Zone NP11 (Lourens et al., 2005; Agnini et al., 2007). A distinct carbonate-poor red clay layer, termed the Elmo horizon, is located within the H1-CIE. Benthic foraminiferal diversity is low in this Elmo horizon and assemblages are dominated by small *Nuttallides truempyi* and *Abyssamina* spp. (Lourens et al., 2005). The slightly younger H2 isotope event appears to be an associated "minor" hyperthermal with a CIE of -0.8‰ and 2 °C warming (Stap et al., 2010). Un-

til now, documentation of ETM-2 in other areas is still quite sparse, hampering assessment of its global biotic impact.

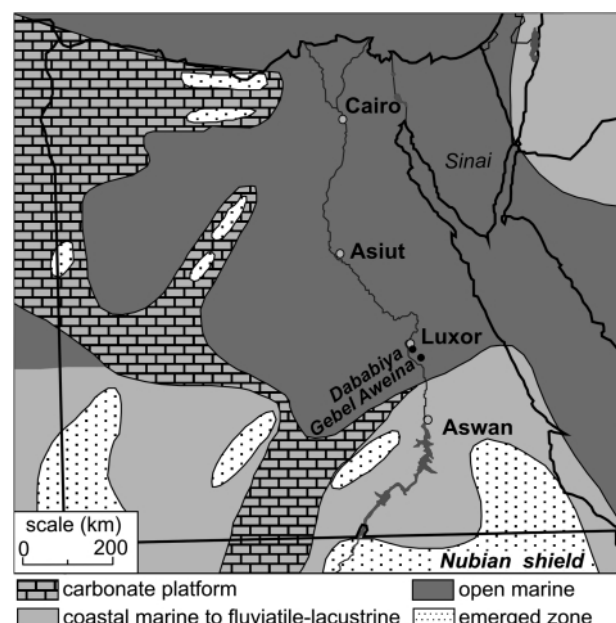


FIGURE 1: Location map of the Dababiya and Gebel Aweina sections, superimposed on a paleogeographic reconstruction of the early Paleogene (modified after Guiraud and Bosworth, 1999).

In Egypt, lower Paleogene sequences are well known and especially the stratigraphy of the Paleocene/Eocene transition has been intensively studied with particular focus on the regional expression of the PETM (e.g. Speijer et al., 2000; Ouda and Berggren, 2003). During the early Paleogene, this area was covered by an epicontinental sea with open connections to the Tethyan Ocean (Fig. 1). At Dababiya, an expanded lower Paleogene sequence is well exposed and the GSSP of the base of the Ypresian and the Eocene is located here (Dupuis et al., 2003; Aubry et al., 2007). The upper Paleocene-lower Eocene interval is represented by the Esna Formation (shaly marls), which is intercalated between the upper Paleocene Tarawan Formation (chalks and limestones) and the lower Eocene Thebes Formation (limestones). The PETM interval deviates from background deposits and is subdivided into 5 beds, called the Dababiya Quarry beds (DQ-beds, Dupuis et al., 2003), revealing the progression of environmental changes during the PETM (Ernst et al., 2006). The upper part of the Dababiya outcrop

(DBD subsection of Dupuis et al., 2003) is stratigraphically well constrained and offers excellent opportunities to investigate ETM-2 in a shelf setting. Here we discuss preliminary results of ETM-2 in a comparison with the PETM and long-term regional trends.

2. MATERIAL AND METHODS

Samples were obtained from two parallel trenches at Dababiya (DBD'06 and high-resolution DBY'09 sample set), spanning the NP10/11 transition at Dababiya. The base (DBD'06 0.0 m) and top (DBD'06 18.0 m) of this sampled interval (Figs. 2 and 3) correspond to the DBD 62.75-82.0 m interval previously described by Dupuis et al. (2003). A calcareous nannofossil investigation was carried out using standard procedures as described in Steurbaut and King (1994). About two square centimeters of glass-slide have been examined for each sample analyzed, using a Zeiss light microscope at 1000x or 1250x magnification. Microfossil residues were obtained following conventional washing procedures (e.g. Ernst et al., 2006).

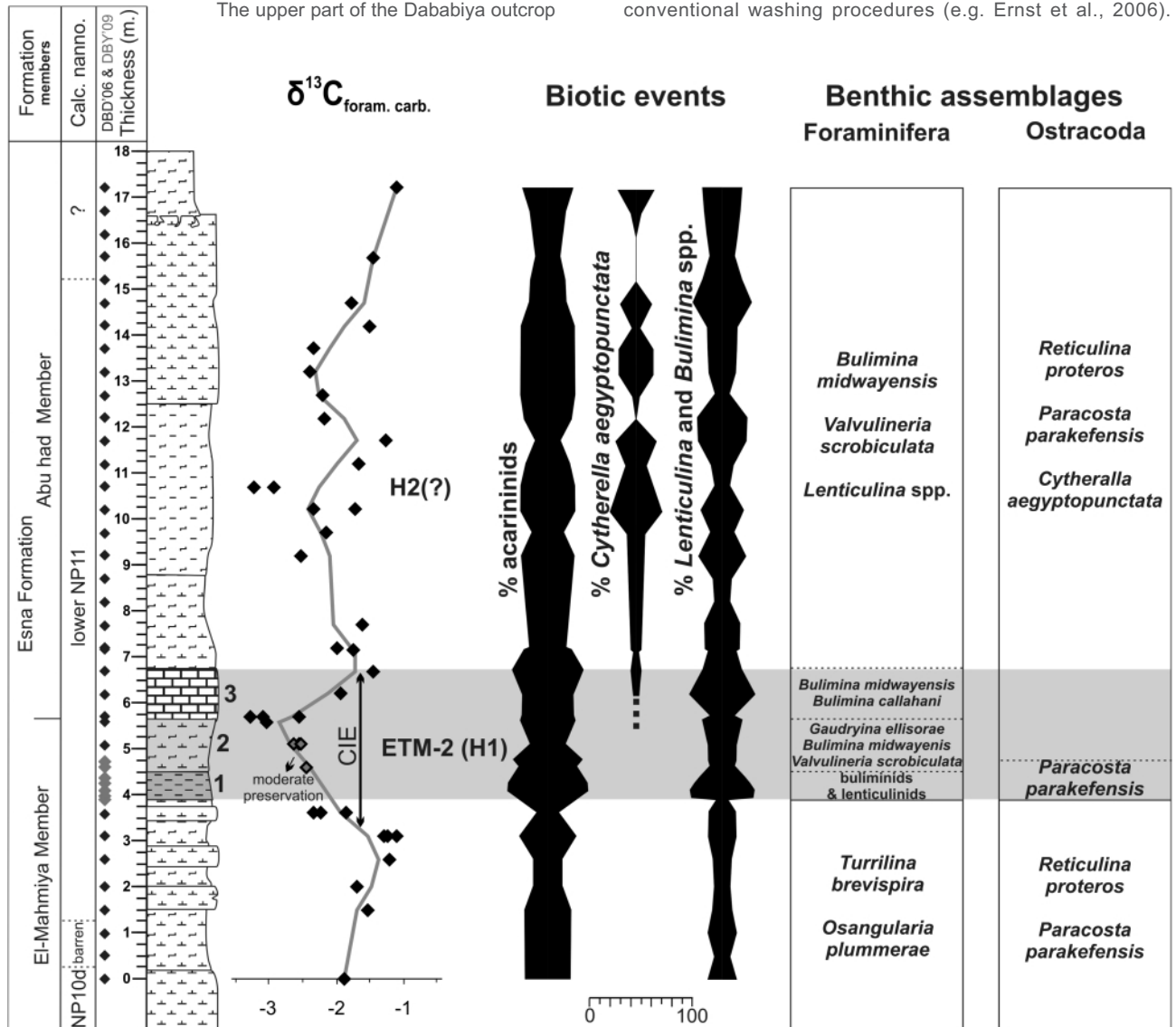


FIGURE 2: Summary of the $\delta^{13}\text{C}$ and biotic record of ETM-2 at Dababiya, Egypt. The gray-shaded area represents the interval with deviating sedimentary features. The $\delta^{13}\text{C}$ record is based on well preserved *Pyramidulina affinis* specimens (gray line ~ 3 point average). Relative abundances of some selected taxa indicate environmental shifts (% acarininids/total planktic foraminifera; % *C. aegyptopunctata*/total ostracodes; % (*Lenticulina* and *Bulimina* species)/total benthic foraminifera).

Compositional foraminiferal data were obtained from the 125-630 μm fraction, whereas ostracodes were retrieved from the $>250 \mu\text{m}$ fraction. The benthic foraminiferal $\delta^{13}\text{C}$ record is based on fragments of single specimens of the thick-shelled *Pyramidulina affinis*. Preservation of the test wall is in general excellent as evaluation by scanning electron microscopy revealed original shell structures with pore canals and the absence

of attached secondary cements (Fig. 4). Only diagenetic infillings of the central voids were detected, those were separated by crushing and selective hand-picking. Carbon isotope analyses were performed with a Kiel III carbonate preparation line, connected to a ThermoFinnigan 252 mass spectrometer at the University of Erlangen. All values are reported in permil relative to V-PDB and analytic reproducibility was better than $\pm 0.01\text{‰}$ (1σ).

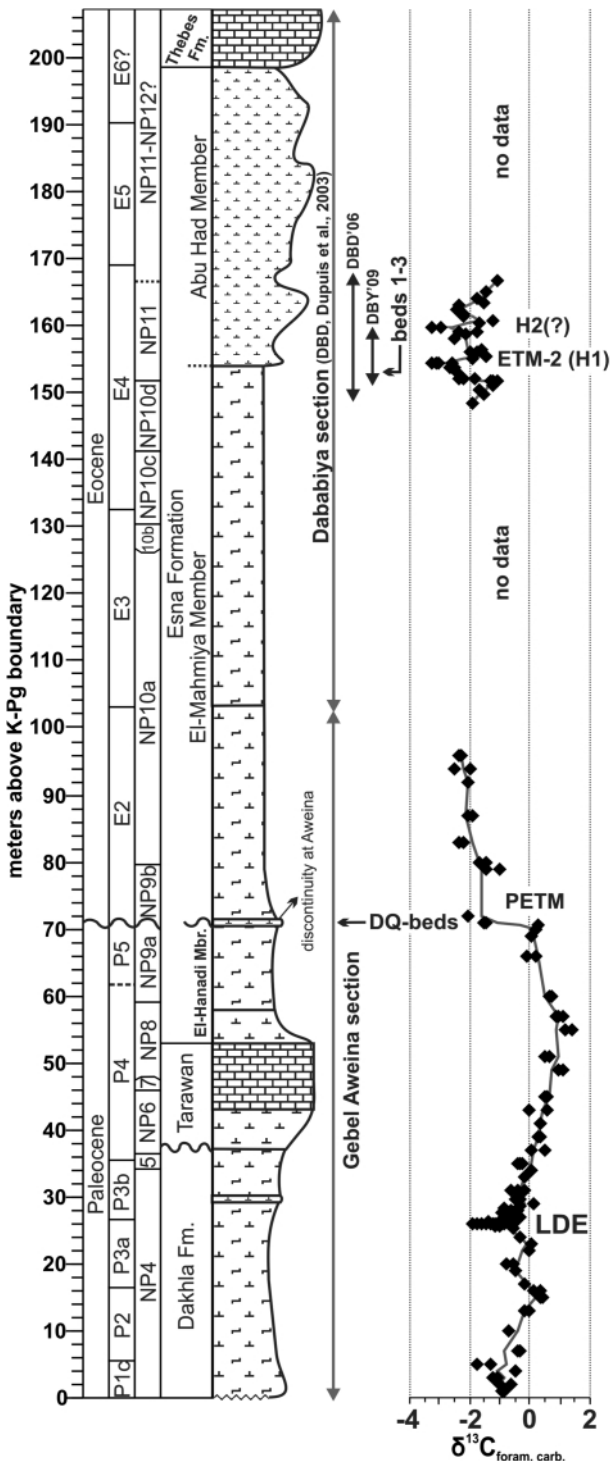


FIGURE 3: Composite section (Gebel Aweina and Dababiya) with a compiled $\delta^{13}\text{C}_{\text{foram. carb.}}$ record (*Pyramidulina* spp.) of the lower Paleocene of Egypt (Paleocene and lowermost Eocene data from Charisi and Schmitz, 1998; Speijer and Schmitz, 1998; Bornemann et al., 2009).

3. RESULTS

3.1 LITHOLOGY

The studied sequence can be divided into three lithologic intervals. The predominant lithology of the lower interval (base to 3.9 m) consists of shaly marls, intercalated by thin marly limestone beds (Fig. 2). The overlying interval (3.9-6.75 m) consists at the base of non-laminated brownish shales (3.9-4.5 m) with occasionally hematitic molds of bivalves, very few fish remains and rare coprolites. It is succeeded by light brown marls (4.5-5.65 m), overlain by a whitish foraminifera-rich chalky limestone bed (5.65-6.75 m). These succeeding lithologies are referred to as beds 1 to 3 and stand out compared to background sediments. The upper marly interval (6.75 m to top) has a lighter color and higher carbonate content. The base of the prominent white chalky limestone bed was chosen to define the boundary between the El-Mahmiya and Abu Had Members of the Esna Formation as this most conspicuous limestone bed can be easily traced between outcrops (DBD 69.5 m; Dupuis et al., 2003; Aubry et al., 2007).

3.2 ISOTOPES

Pyramidulina species have been successfully used for generating $\delta^{13}\text{C}$ records in the epicontinental sequences in Egypt (e.g. Charisi and Schmitz, 1998; Bornemann et al., 2009). Mean stable carbon isotope values of *Pyramidulina affinis* specimens in the studied interval are in the order of -1.9‰ (excluding the interval between 3.9 and 6.75 m). Values are quite stable in the lowest interval (0-3.1 m) with mean values of -1.4‰ (Fig. 2). A distinct negative trend starts at 3.1 m to reach lowest values at the base of the chalky limestone bed at 5.7 m (min. -3.3‰ and mean value -3.0‰). The brownish shales are barren in large-sized foraminifera and the brownish marls yielded only moderately preserved specimens (partial dissolution and hematite staining) with relatively low values. This indicates a CIE of approximately 1.6‰ encompassing the brownish shales. A second negative shift of 1‰ occurs at 10.7 m.

3.3 BIOSTRATIGRAPHY

Two distinct calcareous nannofossil assemblages have been identified in the studied section, separated by a 1 m thick barren interval (0.25-1.25 m, Fig. 2). The lowermost assemblage at the base of the section (0 m) is marked by the co-occurrence of *Tribrachiatus contortus* and *Tribrachiatus orthostylus*, indicating the top of nannofossil Zone NP10 (subzone NP10d). The upper assemblage, ranging from 1.50 m to around 15.20 m,

is characterized by the presence of *Tribrachiatulus orthostylus*, *Discoaster diastypus*, *Discoaster multiradiatus* (up to 14.70 m) and *Ellipsolithus macellus*. The co-occurrence of these taxa, in association with the absence of *T. contortus*, points to the lower part of NP11 (e.g. Steurbaut, 1998; Agnini et al., 2007). The associations in the topmost 2 m of the studied section are substantially recrystallized, hampering an accurate biozonal subdivision. From the foregoing it is clear that the limestone bed at the base of the Abu Had Member, generating the most negative carbon isotope values, is situated within the basal part of zone NP11. This is in accordance with the earlier placement of the base of the Abu Had Member slightly above the NP10-NP11 zonal boundary (Dupuis et al., 2003). It also appears that the second negative carbon isotope excursion, about 5 m higher up, is still within the lower part of NP 11.

3.4 BIOTIC CHANGES

A local benthic turnover is recorded at the base of the brownish shales where a diverse *Turritina brevispira* and *Osangu-laria plummerae* benthic foraminiferal assemblage is rapidly replaced by a less diverse fauna, mainly composed of buliminids and lenticulinids (Figs. 2 and 5). The brownish shales (bed 1) yield a poorly diverse benthic assemblage, dominated by lenticulinids, *Bulimina ovata* and *Bulimina midwayensis*. Many foraminiferal tests within bed 1 are poorly preserved and contain hematite grains or staining (Fig. 5). These hematite grains resemble biogenic pyrite framboids. We therefore attribute the poor preservation to weathering of pyrite-filled tests. The brownish marls (bed 2) contain a somewhat more diverse benthic assemblage of which the major components are *Valvulineria scrobiculata*, *Gaudryina ellisorae* and *B. midwayensis*. The diversity of the benthic assemblages within the white chalky limestone bed is as high as in the lowermost marly interval (0-3.9 m) and the major components are *Bulimina callahani* and *B. midwayensis*. The assemblage above bed 3 is dominated by *B. midwayensis*, *V. scrobiculata* and *Lenticulina* spp. *Gaudryina ellisorae* remains a continuous minor component. The overall biotic turnover across the studied interval is limited.

Planktic-Benthic ratios (P/B) are high within the whole sequence (> 80%, excluding taphonomically altered beds). Slightly higher P/B and a significant increase of *Acarinina* species in the planktic foraminiferal assemblage are observed between 3.9 and 6.75 m. A less pronounced ostracode assemblage change is also recorded within this interval, marked by a common occurrence of *Cytherella aegyptopunctata* from the base of the limestone bed upwards (Fig. 2). This ostracode species is until now only recorded within and

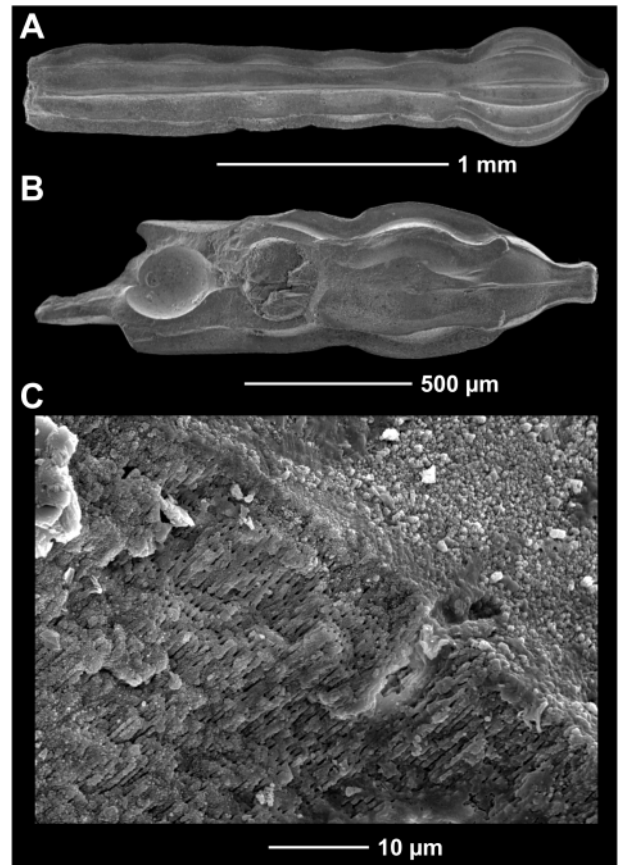


FIGURE 4: Scanning electron micrographs of *Pyramidulina affinis* (d'Orbigny). A: entire specimen, B: broken specimen with a removable diagenetic chamber infilling, C: detail of test wall displaying well-preserved original shell structure with pore canals.

just above the PETM in two neritic sequences in Egypt (Gebel Duwi and Gebel Aweina, Morsi and Speijer, 2003).

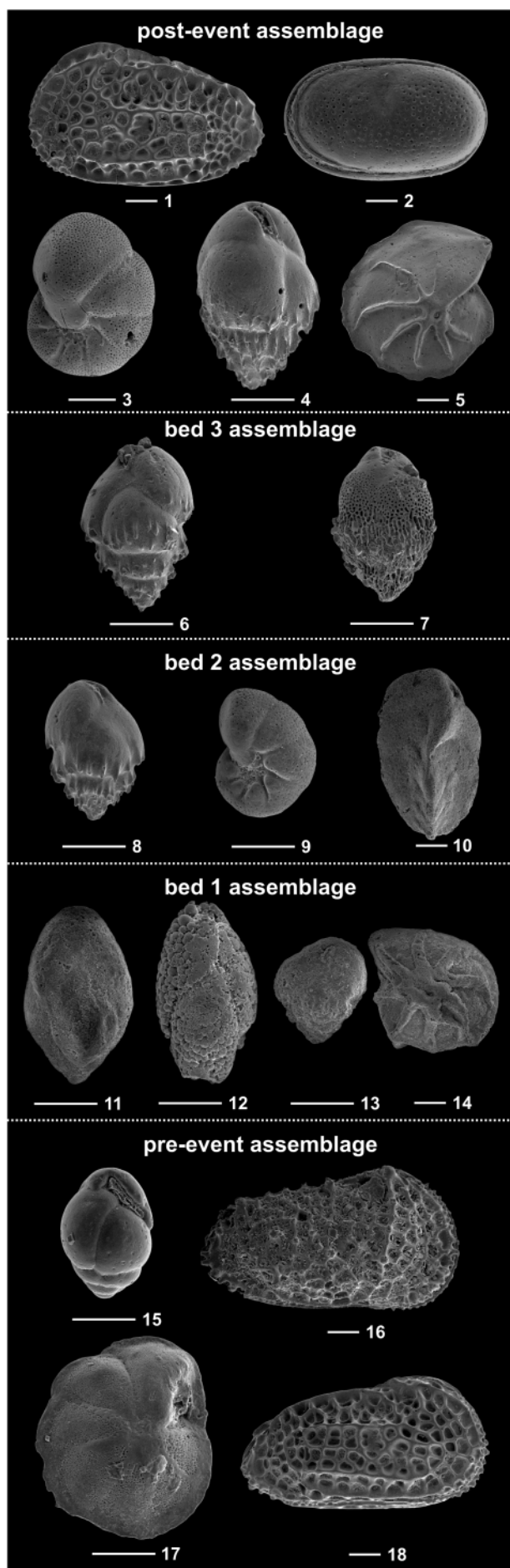
4. DISCUSSION

In general, the diverse benthic assemblages within the lower shaly marl unit indicate a deep shelf environment with well-ventilated bottom water and a moderate organic flux. In the brow-

Parameter	background NP9b-NP11	PETM	ETM-2
carbon isotope excursion	no	yes	yes
predominant lithology	shales-marls	dark shales and marls foram.-rich limestone	dark shales and marls foram.-rich limestone
laminated sediments	no	yes	no
organic enrichment (black shales)	no	yes	yes (minor)
coprolites	rare	abundant	no
fish remains	rare	abundant	rare
P/B (>125 µm)*	60-95%	95-99%	80-95%
<i>Morozovella</i> species	common to abundant	rare	common
<i>Acarinina</i> species	common to abundant	dominant	dominant
benthic diversity drop	no	yes	yes
benthic foraminiferal change	no	yes	yes
ostracode turnover	no	yes	yes
oxygenation sea floor	good to moderate	poor (anoxic-dysoxic)	poor (dysoxic)

*excluding taphonomically altered levels

TABEL 1: Comparison of Egyptian biotic and sedimentary features between ETM-2, PETM and background characteristics, as observed in the Gebel Aweina (Speijer and Schmitz, 1998) and Daba-biya (Ernst et al., 2006; this study) sections.



nisch shales (bed 1), the diversity drops and the blooms of opportunistic buliminids and lenticulinids point to oxygen stress (dysoxia) at the sea floor during deposition of bed 1, whereas the dominance of acarininids indicates that also the surface mixed layer was affected. The presence of pyrite suggests anoxic-dysoxic conditions within the sediment although not fully extending to the sediment surface as indicated by the continuous presence of endobenthic taxa (buliminids). Assemblages of bed 2 are slightly more diverse, yet still dominated by endobenthic species, indicating the continuation of low-oxygen conditions. The foraminifera-rich chalky limestone bed and the upper marly interval represent the return of well-ventilated bottom water with a moderate to high organic flux, as indicated by increased diversity and high proportion of lenticulinids and buliminids.

This biotic record indicates a sudden paleoenvironmental perturbation within the basal part of the NP11 interval in association with a CIE of approximately 1.6‰. Negative $\delta^{13}\text{C}$ anomalies of this magnitude in the Egyptian basin are only recorded at older hyperthermal events (PETM and LDE, Fig. 3). Based on the stratigraphic position and magnitude of the CIE, we assign this environmental perturbation to ETM-2 and the H1 isotope event. The onset of the CIE starts below the base of the brownish shales. Similar patterns are observed in the deep-sea (Walvis Ridge) where the onset of the CIE precedes the clay-rich Elmo horizon (Stap et al., 2010). The second CIE of 1‰ is situated within the lower part of Zone NP11 and probably represents the H2 event. No biotic or lithologic changes are associated with this level.

This proposed ETM-2 event bears similarity in biotic and sedimentary features with the PETM at Dababiya and deviates from background characteristics of the Egyptian Basin (Table 1). Both the PETM and ETM-2 are marked by the sudden expansion of low-oxygen conditions and the establishment of peculiar planktic and benthic assemblages. Yet, the oxygen restriction during ETM-2 was less severe as sediments are not laminated with less accumulation of organic material. Secondly, the ETM-2 beds contain an impoverished benthic fauna whereas the lower PETM beds at Dababiya are devoid of

FIGURE 5: Representative species of the Dababiya ETM-2 sequence (scale bar represents 100 μm and sample origin is given between brackets). 1) *Paracosta kefensis* (Benson) (DBD'06 11.7 m); 2) *Cytherella aegyptopunctata* Morsi & Speijer (DBD'06 12.5 m); 3) *Valvulineria scrobiculata* (Schwager) (DBD'06 10.94 m); 4) *Bulimina midwayensis* Cushman & Parker (DBD'06 10.94 m); 5) *Lenticulina* sp. (DBD'06 10.94 m); 6) *Bulimina midwayensis* Cushman & Parker (DBD'06 6.13 m); 7) *Bulimina callahani* Galloway and Morrey (DBD'06 6.13 m); 8) *Bulimina midwayensis* Cushman & Parker (DBD'06 5.16 m); 9) *Valvulineria scrobiculata* (Schwager) (DBD'06 5.16 m); 10) *Gaudryina ellisorae* Cushman (DBD'06 5.16 m); 11) *Bulimina ovata* d'Orbigny (DBD'06 3.96 m); 12) *Bulimina ovata* d'Orbigny (specimen with hematite infilling, DBD'06 3.96 m); 13) *Bulimina midwayensis* Cushman & Parker (partly dissolved, DBD'06 3.96 m); 14) *Lenticulina* sp. (partly dissolved, DBD'06 3.96 m); 15) *Turrilina brevispira* ten Dam (DBD'06 2.52 m); 16) *Reticulina proteros* Bassiouni (DBD'06 2.52 m); 17) *Osangularia plummerae* Brotzen (DBD'06 2.52 m); 18) *Paracosta kefensis* (Benson) (DBD'06 2.52 m)

benthic life (anoxic bottom conditions). Both events triggered long-term biotic assemblage changes in the foraminiferal and ostracod communities and a long-lasting bulminid bloom. Additionally, the distribution patterns of *Turrilina brevispira*, *Gaudryina ellisorae* and *Cytherella aegyptopunctata* are remarkable. *Turrilina brevispira* became a common component of benthic assemblages in the aftermath of the PETM (Speijer and Schmitz, 1998; Ernst et al., 2006) and almost entirely disappears at the onset of ETM-2. Therefore the highest common occurrence of *T. brevispira* could potentially be used as a local (to regional?) marker species for the ETM-2 interval. *Cytherella aegyptopunctata* first appears within the PETM interval in the Gebel Duwi and Gebel Aweina sections (Morsi and Speijer, 2003) and the reappearance of this characteristic species may be used as an additional regional marker. *Gaudryina ellisorae* sporadically occurs below ETM-2 and becomes a common species from bed 2 onwards. This distribution resembles the record of the similar *Gaudryina cf. ellisorae*, which has its first occurrence within the PETM interval at Dababiya and Aweina (Speijer and Schmitz, 1998; Ernst et al., 2006).

The lithologic sequence of the ETM-2 interval resembles to some degree the Dababiya Quarry beds (DQ-beds, Dupuis et al., 2003). The brownish shales and light brown marls (bed 1 and 2) seem comparable to DQ-beds 1-4, although an accumulation of coprolites or lamination is absent. The whitish foraminifera-rich chalky limestone (bed 3) strongly resembles DQ-bed 5. Both chalky limestone beds contain abundant foraminifera, a restored benthic fauna and a dominance of *Bulimina callahani* and both beds are situated in the final recovery phase of a CIE. The accumulation of foraminifera within DQ-bed 5 is interpreted as a condensation interval during highest sea level (maximum flooding surface) with high oxygen levels and moderate organic flux to the sea floor (Ernst et al., 2006). The whitish chalky limestone bed (bed 3) in our studied interval may represent a similar feature.

All these similarities point to analogous processes operating in the Egyptian Basin during these hyperthermals, although the overall environmental impacts differ in magnitude. During the early Eocene, prevailing mesotrophic conditions changed into eutrophic dysoxic conditions during the early part of ETM-2 as the net result of increased temperature and disruption of the basin circulation patterns. Fully anoxic or suboxic conditions were never established, yet the environmental perturbation was severe enough to trigger long-lasting biotic assemblage changes in this area, reappearance of a specialized ostracod species and increased abundances of calcareous agglutinated benthic foraminifera. During ETM-2, the lysocline in the deep-sea recovered within 30 kyr, followed by a period of carbonate oversaturation (Stap et al., 2009). The white chalky limestone (bed 3) may represent this period of excess carbonate sedimentation. Additional studies are needed to evaluate the regional significance of the observed patterns and to provide a model linking these to the paleoclimatic and paleoceanographic changes.

5. CONCLUSIONS

Our preliminary data provide the first evidence of ETM-2 in a shelf sequence and its consequences on a shallow marine ecosystem. Similar to the PETM at Dababiya, ETM-2 reveals anomalous sedimentologic features and corresponding changes in benthic and planktic foraminifera as well as in ostracodes. These biotic shifts indicate a temporary perturbation of the complete marine ecosystem with some long-term compositional adjustments in benthic communities. Yet, unlike to the PETM, a complete collapse of the benthic ecosystem did not occur as critical oxygen conditions (anoxia) were absent.

ACKNOWLEDGEMENTS

We thank Mohammed Youssef (South Valley University, Qena) for assistance in the field. Financial support was provided by grants from the KU Leuven Research Fund and the Research Foundation Flanders (FWO) to Robert P. Speijer and Etienne Steurbaut. We thank Bettina Schenk and an anonymous reviewer for constructive reviews.

REFERENCES

- Agnini, C., Fornaciari, E., Raffi, I., Rio, D., Röhl, U. and Westerhold, T., 2007. High-resolution nannofossil biochronology of middle Paleocene to early Eocene at ODP Site 1262: Implications for calcareous nannoplankton evolution. *Marine Micropaleontology*, 64, 215-248.
- Aubry, M.-P., Ouda, K., Dupuis, C., Berggren, W.A., Van Couvering, J.A., Ali, J., Brinkhuis, H., Gingerich, P.D., Heilmann-Clausen, C., Hooker, J., Kent, D.V., King, C., Knox, R., Laga, P., Molina, E., Schmitz, B., Steurbaut, E. and Ward, D., 2007. The global Standard Stratotype-section and Point (GSSP) for the base of the Eocene Series in the Dababiya section (Egypt). *Episodes*, 30, 271-286.
- Bornemann, A., Schulte, P., Sprong, J., Steurbaut, E., Youssef, M. and Speijer, R.P., 2009. Latest Danian carbon isotope anomaly and associated environmental change in the southern Tethys (Nile Basin, Egypt). *Journal of the Geological Society*, 166, 1135-1142.
- Charisi, S.D. and Schmitz, B., 1998. Paleocene to early Eocene paleoceanography of the Middle East: The $\delta^{13}\text{C}$ and $\delta^{18}\text{O}$ isotopes from foraminiferal calcite. *Paleoceanography*, 13, 106-118.
- Cramer, B.S., Wright, J.D., Kent, D.V. and Aubry, M.P., 2003. Orbital climate forcing of $\delta^{13}\text{C}$ excursions in the late Paleocene-early Eocene (chrons C24n-C25n). *Paleoceanography*, 18, PA1097.

- Dupuis, C., Aubry, M.-P., Steurbaut, E., Berggren, W.A., Ouda, K., Magioncalda, R., Cramer, B.S., Kent, D.V., Speijer, R.P. and Heilmann-Clausen, C., 2003. The Dababiya Quarry section: Lithostratigraphy, clay mineralogy, geochemistry and paleontology. *Micropaleontology*, 49, 41-59.
- Ernst, S.R., Guasti, E., Dupuis, C. and Speijer, R.P., 2006. Environmental perturbation in the southern Tethys across the Paleocene/Eocene boundary (Dababiya, Egypt): Foraminiferal and clay mineral records. *Marine Micropaleontology*, 60, 89-111.
- Guiraud, R. and Bosworth, W., 1999. Phanerozoic geodynamic evolution of northeastern Africa and the northwestern Arabian platform. *Tectonophysics*, 315, 73-108.
- Lourens, L.J., Sluijs, A., Kroon, D., Zachos, J.C., Thomas, E., Röhl, U., Bowles, J. and Raffi, I., 2005. Astronomical pacing of late Palaeocene to early Eocene global warming events. *Nature*, 435, 1083-1087.
- Morsi, A.-M.M. and Speijer, R.P., 2003. High-resolution ostracode records of the Paleocene/Eocene transition in the South Eastern Desert of Egypt - Taxonomy, biostratigraphy, paleoecology and paleobiogeography. *Senckenbergiana lethaea*, 83, 61-93.
- Ouda, K. and Berggren, W.A., 2003. Biostratigraphic correlation of the Upper Paleocene-Lower Eocene succession in the Upper Nile Valley: A synthesis. *Micropaleontology*, 49, 179-212.
- Speijer, R.P. and Schmitz, B., 1998. A benthic foraminiferal record of Paleocene sea level and trophic/redox conditions at Gebel Aweina, Egypt. *Palaeogeography, Palaeoclimatology, Palaeoecology*, 137, 79-101.
- Speijer, R.P., Schmitz, B. and Luger, P., 2000. Stratigraphy of late Palaeocene events in the Middle East: implications for low- to middle-latitude successions and correlations. *Journal of the Geological Society*, 157, 37-47.
- Stap, L., Lourens, L.J., Thomas, E., Sluijs, A., Bohaty, S. and Zachos, J.C., 2010. High-resolution deep-sea carbon and oxygen isotope records of Eocene Thermal Maximum 2 and H2. *Geology*, 38, 607-610.
- Stap, L., Sluijs, A., Thomas, E. and Lourens, L., 2009. Patterns and magnitude of deep sea carbonate dissolution during Eocene Thermal Maximum 2 and H2, Walvis Ridge, southeastern Atlantic Ocean. *Paleoceanography*, 24, PA1211.
- Sturbaut, E., 1998. High-resolution holostratigraphy of Middle Paleocene to Early Eocene strata of Belgium and adjacent areas. *Palaeontographica Abteilung A, Paläozoologie--Stratigraphie*, 247, 91-156.
- Sturbaut, E. and King, C., 1994. Integrated stratigraphy of the Mont-Panisel borehole section (151E340), Ypresian (Early Eocene) of the Mont Basin, SW Belgium. *Bulletin de la Société belge de Géologie - Bulletin van de Belgische Vereniging voor Geologie*, 102, 175-202.
- Westerhold, T., Röhl, U., Donner, B., McCarren, H.K. and Zachos, J.C., 2011. A complete high-resolution Paleocene benthic stable isotope record for the central Pacific (ODP Site 1209). *Paleoceanography*, 26, PA2216.
- Zachos, J.C., Dickens, G.R. and Zeebe, R.E., 2008. An early Cenozoic perspective on greenhouse warming and carbon-cycle dynamics. *Nature*, 451, 279-283.

Received: 18 October 2011

Accepted: 24 February 2012

Peter STASSEN¹⁾, Etienne STEURBAUT¹²⁾, Abdel-Mohsen M. MORSI³⁾, Peter SCHULTE⁴⁾ & Robert P. SPEIJER¹⁾

¹⁾ Department of Earth and Environmental Sciences, KU Leuven, Celestijnenlaan 200E, B-3001, Leuven, Belgium;

²⁾ Department of Paleontology, Royal Belgian Institute of Natural Sciences, Vautierstraat 29, B-1000, Brussels, Belgium;

³⁾ Department of Geology, Faculty of Science, Ain Shams University, 11566 Cairo, Egypt;

⁴⁾ GeoZentrum Nordbayern, Universität Erlangen, Schlossgarten 5a, D-91054 Erlangen, Germany;

^{*)} Corresponding author, peter.stassen@ees.kuleuven.be